ULTRASOUND NEWS

April 2022

Noninvasive assessment of hepatic steatosis using a pathologic reference standard: comparison of CT, MRI, and US-based techniques

Jae Seok Bae[1,2], Dong Ho Lee[1,2], Kyung-Suk Suh[3], Haeryoung Kim[4], Kyung Bun Lee[4], Jae Young Lee[1,2,5], Joon Koo Han[1,2,5]

[1]Department of Radiology, Seoul National University Hospital, Seoul; [2]Department of Radiology, Seoul National University College of Medicine, Seoul; Departments of [3]Surgery and [4]Pathology, Seoul National University Hospital, Seoul; [5]Institute of Radiation Medicine, Seoul National University Medical Research Center, Seoul, Korea

ULTRASONOGRAPHY

ORIGINAL ARTICLE

https://doi.org/10.14366/usg.21150
pISSN: 2288-5919 • eISSN: 2288-5943
Ultrasonography 2022;41:344-354

Received: July 18, 2021
Revised: September 29, 2021
Accepted: October 25, 2021

Correspondence to:
Dong Ho Lee, MD, Department of Radiology, Seoul National University Hospital, 101 Daehak-ro, Jongno-gu, Seoul 03080, Korea

Tel. +82-2-2072-3107
Fax. +82-2-743-6385
E-mail: dhlee.rad@gmail.com

Purpose: The present study compared the performance of computed tomography (CT), magnetic resonance imaging–derived proton density fat fraction (MRI-PDFF), controlled attenuation parameter (CAP), grayscale ultrasonography (US), and attenuation imaging (ATI) for the diagnosis of hepatic steatosis (HS).

Methods: In total, 120 prospectively recruited patients who underwent hepatic resection between June 2018 and June 2020 were retrospectively analyzed. CT, MRI-PDFF, CAP, grayscale US, and ATI were performed within 3 months before surgery. Diagnostic performance for HS ≥5% and HS >33% was compared using the area under the curve (AUC) of receiver operating characteristic curves. Histopathologic examinations served as the reference standard for the degree of HS.

Results: For detecting HS ≥5%, MRI-PDFF (AUC, 0.946) significantly outperformed CT, CAP and grayscale US (AUC, 0.807, 0.829, and 0.761, respectively) ($P<0.01$ for all). ATI (AUC, 0.892) was the second-best modality and significantly outperformed grayscale US ($P=0.001$). In pairwise comparisons, there were no significant differences between the AUC of ATI and the values of MRI-PDFF, CT, or CAP ($P=0.133$, $P=0.063$, and $P=0.150$, respectively). For detecting HS >33%, all the modalities provided good diagnostic performance without significant differences (AUC, 0.887–0.947; $P>0.05$ for all).

Conclusion: For detecting HS ≥5%, MRI-PDFF was the best imaging modality, while ATI outperformed grayscale US. For detecting HS >33%, all five imaging tools demonstrated good diagnostic performance.

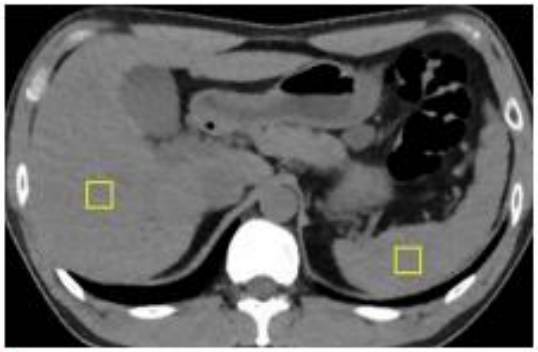

A

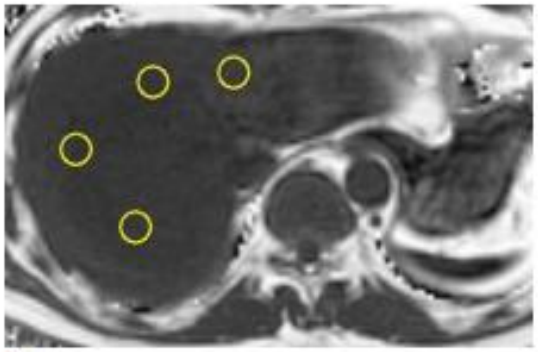

B

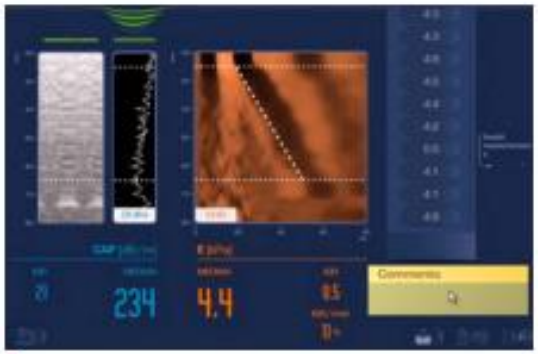

C

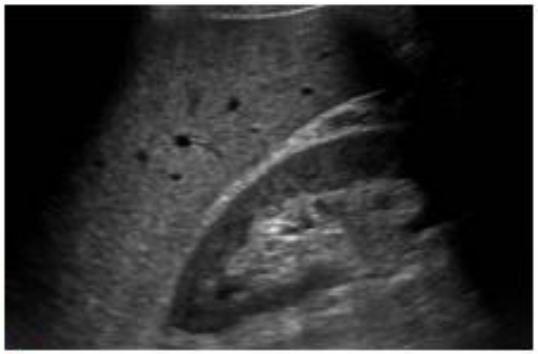

D

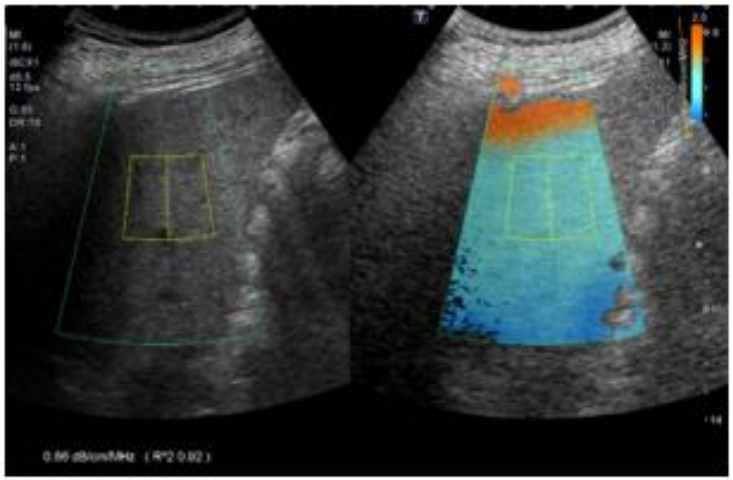

E

Fig. 2. **Representative examples of the findings obtained using noninvasive tools in a 53-year-old man.**

A. On unenhanced axial computed tomography images, 1.5×1.5-cm regions of interest (ROIs) (yellow squares) were placed in the liver and spleen. B. On a proton density fat fraction map of magnetic resonance imaging, 1×1 cm ROIs (yellow circles) were placed in each Couinaud segment of the liver. C. The controlled attenuation parameter was obtained from transient elastography. D. On grayscale ultrasound images, the echogenicity of the hepatic parenchyma was compared with that of the right kidney. E. Attenuation imaging was performed to measure the attenuation coefficient. On pathologic examination, the degree of hepatic steatosis was ≥5%–33%.

Comparison of superb microvascular imaging and shear wave elastography for assessing liver fibrosis in chronic hepatitis B

Mesude Tosun, Hande Uslu

Department of Radiology, Kocaeli University School of Medicine, Kocaeli, Turkey

ULTRA SONO GRAPHY

ORIGINAL ARTICLE

https://doi.org/10.14366/usg.21136
pISSN: 2288-5919 • eISSN: 2288-5943
Ultrasonography 2022;41:394-402

Purpose: The present study investigated the effectiveness and applicability of superb microvascular imaging (SMI) in determining the degree of liver fibrosis noninvasively in comparison with shear wave elastography (SWE).

Methods: Ninety-eight consecutive patients with chronic hepatitis B who underwent ultrasound (US)-guided needle biopsy were examined using US combined with SMI and SWE. The predictive performance of the two US techniques in staging liver fibrosis and inflammation was compared with reference to the histological findings obtained from liver biopsy. The intraobserver and interobserver reproducibility of SMI in vascularity scores were evaluated.

Results: SWE values and SMI vascular scores were statistically significantly different among fibrosis stages ($\chi^2(3)=76.3$, $\chi^2(3)=81.5$, $P<0.001$). The SWE and SMI models significantly predicted fibrosis stages separately, and SMI scores alone predicted fibrosis stages better than SWE values (50.1% for SWE, 63.5% for SMI, $P<0.001$). A model with both SMI scores and SWE values together explained 73.2% of variance in fibrosis stages. When other clinical and laboratory predictors were added to the model (81.5%, $P<0.001$), SWE values and SMI scores remained the main predictors of fibrosis stages. SWE and SMI were also applicable in predicting inflammatory grades, explaining 31% and 34% of variance, respectively, and 37.7% when used together ($P<0.001$).

Conclusion: Both SWE and SMI had good diagnostic performance in determining the degree of liver fibrosis in chronic hepatitis B patients. The efficacy of SMI was better than that of SWE. SMI can improve diagnostic performance for staging liver fibrosis and shows potential for estimating necroinflammation of the liver.

Received: June 23, 2021
Revised: November 15, 2021
Accepted: November 25, 2021

Correspondence to:
Mesude Tosun, MD, Department of Radiology, Kocaeli University Faculty of Medicine, 41380 Kocaeli, Turkey

Tel. +90-262-303-7575
Fax. +90-262-303-7001
E-mail: mesudetosun@hotmail.com, mesude.tosun@kocaeli.edu.tr

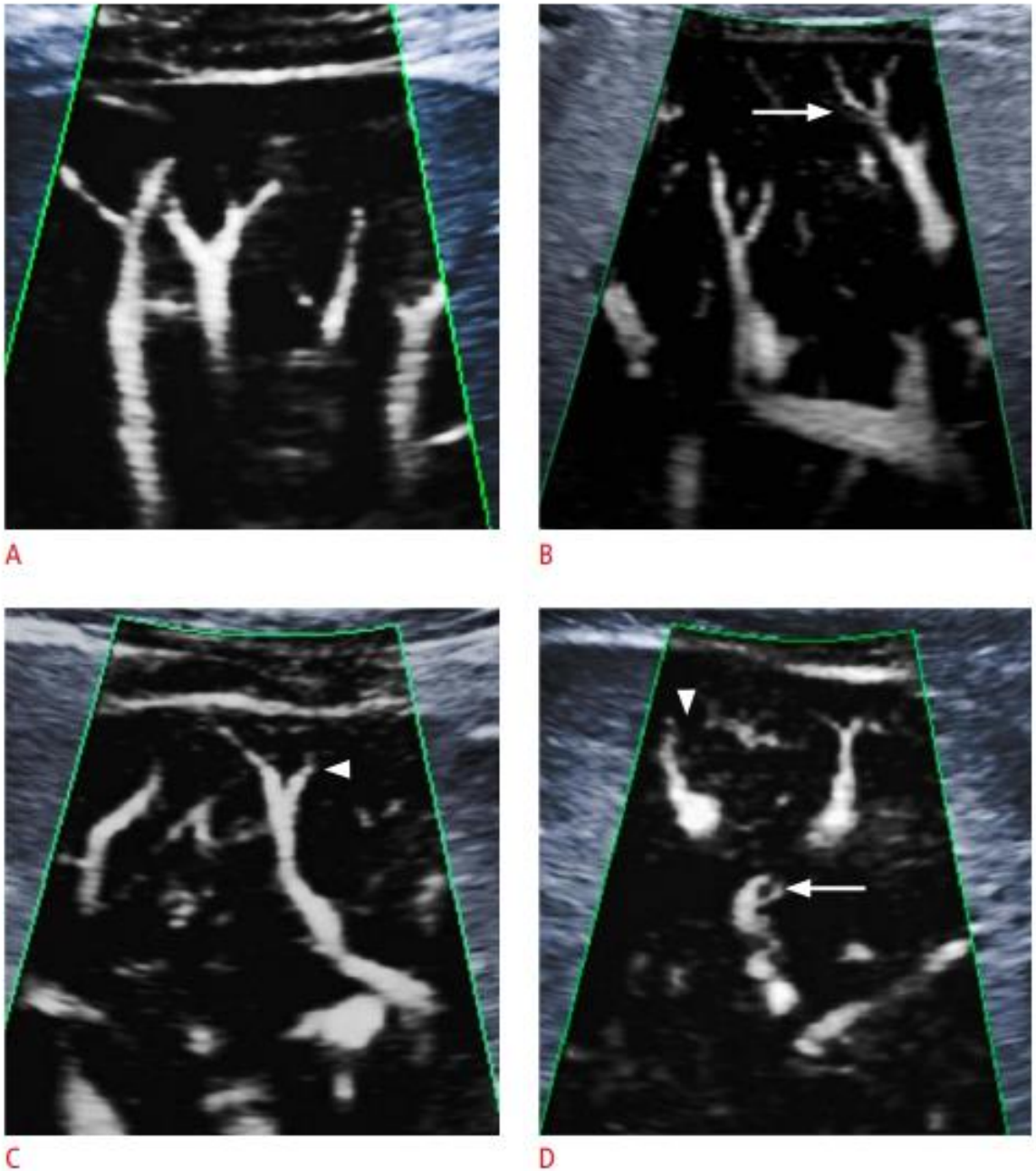

Fig. 1. Superb microvascular imaging vascular scores.
A, D. Superb microvascular imaging (SMI) images at different fibrosis stages are shown. A. This figure (monochrome SMI) shows thinning of the distal branches but no evidence of tortuosity or blunting, classified as a vascular score of 1 according to Doppler grading. B. This figure shows tortuosity (arrow) in distal branches but no evidence of blunting, classified as a vascular score of 2. C. Monochrome SMI image shows blunting in small branches (arrowhead) but not in large branches, classified as a vascular score of 3. D. Monochrome SMI image shows tortuosity, blunting in small (arrow) and large branches (arrowhead), classified as a vascular score of 4.

Conclusion

SWE and SMI models significantly predicted fibrosis stages, with SMI scores alone showing better predictive power than SWE values alone. Considering these results, the authors suggest that SMI, like SWE, can be widely used in the evaluation of liver fibrosis in patients with chronic liver disease. These techniques can improve the diagnostic performance of conventional US and can be useful in the accurate assessment of liver fibrosis stages; therefore, they may be able to contribute to follow-up of these patients in daily practice.

ORCID: Mesude Tosun: https://orcid.org/0000-0

Speckle tracking ultrasonography as a new tool to assess diaphragmatic function: a feasibility study

Sebastian Johannes Fritsch[1], Nima Hatam[2], Andreas Goetzenich[2], Gernot Marx[1], Rüdiger Autschbach[2], Leo Heunks[3], Johannes Bickenbach[1]*, Christian Simon Bruells[4]*

Departments of [1]Intensive Care Medicine and [2]Thoracic and Cardio-Vascular Surgery, University Hospital RWTH Aachen, Aachen, Germany; [3]Department of Intensive Care Medicine, Amsterdam UMC, Vrije Universiteit Amsterdam, Amsterdam, The Netherlands; [4]Department of Anesthesiology, University Hospital RWTH Aachen, Aachen, Germany

ULTRA SONO GRAPHY

TECHNICAL NOTE

https://doi.org/10.14366/usg.21044
pISSN: 2288-5919 • eISSN: 2288-5943
Ultrasonography 2022;41:403-415

A reliable method of measuring diaphragmatic function at the bedside is still lacking. Widely used two-dimensional (2D) ultrasonographic measurements, such as diaphragm excursion, diaphragm thickness, and fractional thickening (FT) have failed to show clear correlations with diaphragmatic function. A reason for this is that 2D ultrasonographic measurements, like FT, are merely able to measure the deformation of muscular diaphragmatic tissue in the transverse direction, while longitudinal measurements in the direction of contracting muscle fibres are not possible. Speckle tracking ultrasonography, which is widely used in cardiac imaging, overcomes this disadvantage and allows observations of movement in the direction of the contracting muscle fibres, approximating muscle deformation and the deformation velocity. Several studies have evaluated speckle tracking as a promising method to assess diaphragm contractility in healthy subjects. This technical note demonstrates the feasibility of speckle tracking ultrasonography of the diaphragm in a group of 20 patients after an aortocoronary bypass graft procedure. The results presented herein suggest that speckle tracking ultrasonography is able to depict alterations in diaphragmatic function after surgery better than 2D ultrasonographic measurements.

Keywords: Diaphragm; Ultrasonography; Speckle tracking ultrasound; Fractional thickening

Key points: A reliable sonographic measurement method for bedside assessment of

Received: February 25, 2021
Revised: August 16, 2021
Accepted: August 17, 2021

Correspondence to:
Sebastian Johannes Fritsch, MD, Department of Intensive Care Medicine, University Hospital RWTH Aachen, Pauwelsstr. 30, 52074 Aachen, Germany

Tel. +49-241-8080444
Fax. +49-241-803380444
E-mail: sfritsch@ukaachen.de

*These authors contributed equally to this work.

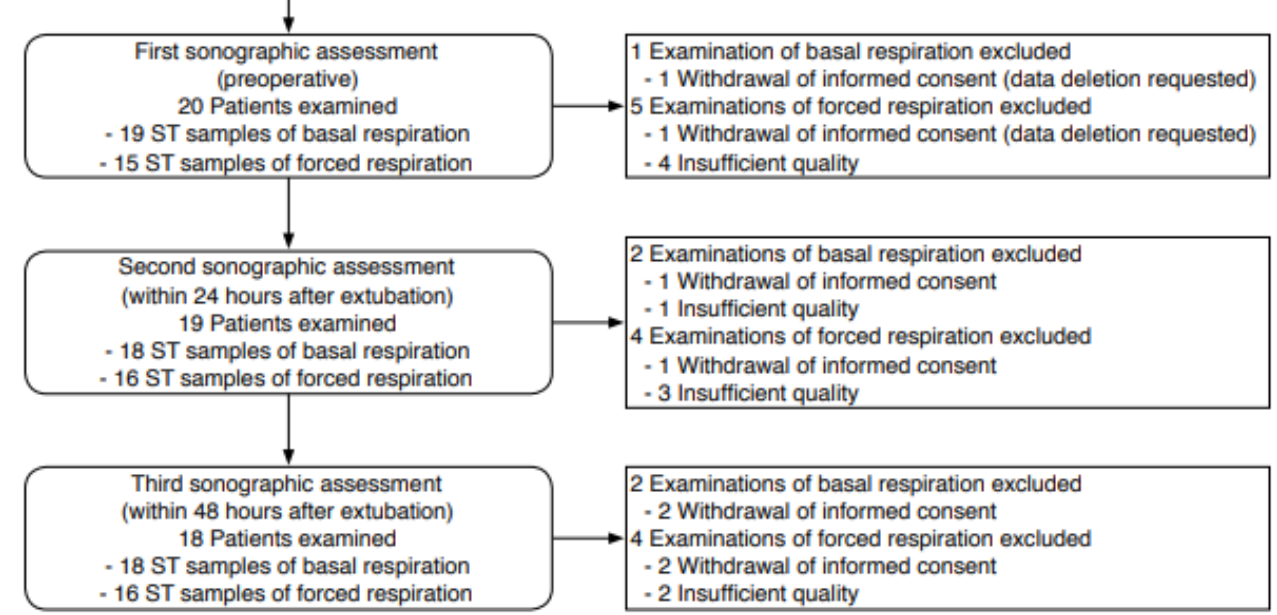

Fig. 1. Flowchart of the patient population. The flowchart shows the course of examined patient numbers in the present feasibility study over time. Additionally, it shows the number of patients excluded with the respective reasons. CABG, coronary artery bypass graft; ST, speckle tracking.

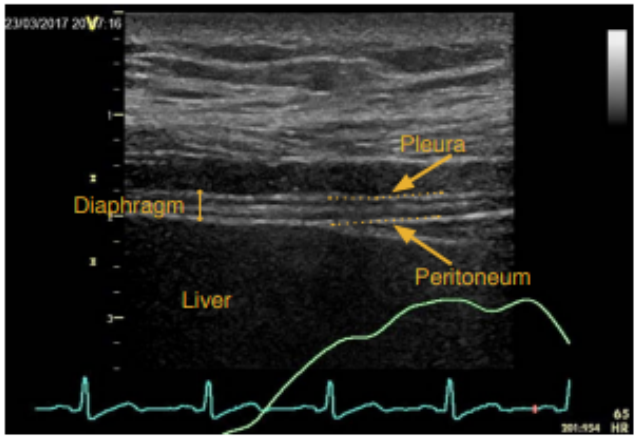

Fig. 2. Ultrasonographic imaging of the diaphragm recorded in B-mode in the zone of apposition. The diaphragm is displayed between the two echogenic lines above the liver tissue, which represent the pleura and peritoneum.

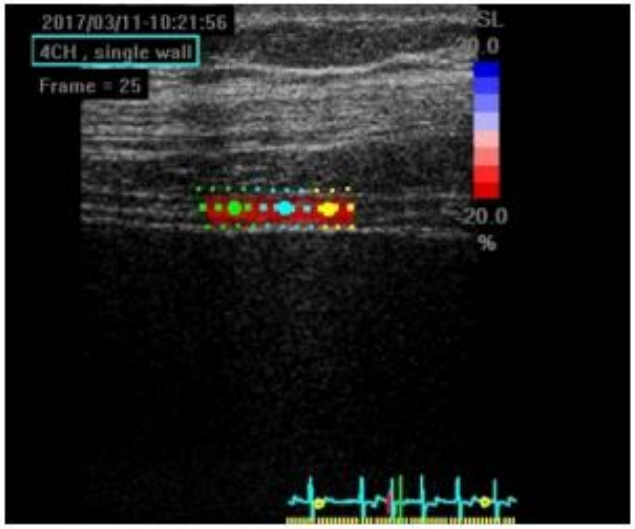

A

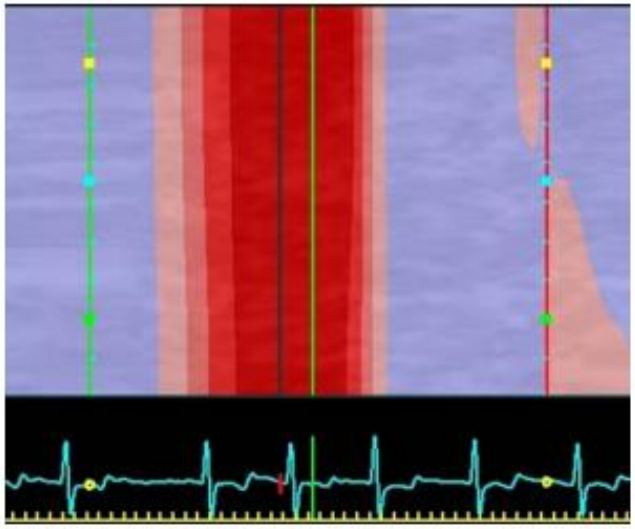

B

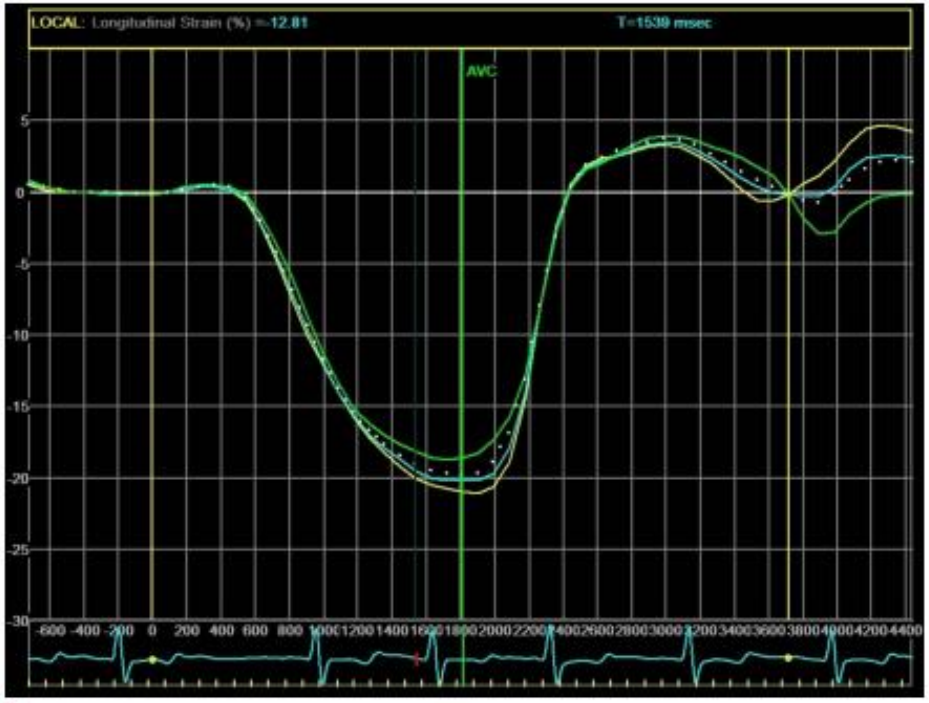

C

Fig. 3. A screenshot of the Q-analysis tool of the EchoPac software.
A. The subscreen shows a B-mode picture of the diaphragm with the respective regions of interest. B. This diagram visualizes contraction in relation to time (x-axis) and localization in the respective region of interest (ROI) (y-axis). C. The main graphs represent the strain values of the different ROIs over the course of one breathing cycle.

Ultrasonographic atlas of splenic lesions

Gayoung Choi[1,2], Kyeong Ah Kim[1], Jinhwan Lee[3], Yang Shin Park[1], Jongmee Lee[1], Jae Woong Choi[1], Chang-Hee Lee[1]

[1]Department of Radiology, Korea University Guro Hospital, Korea University College of Medicine, Seoul; [2]Department of Radiology, Korea University Ansan Hospital, Korea University College of Medicine, Ansan; [3]Department of Pathology, Korea University Guro Hospital, Korea University College of Medicine, Seoul, Korea

ULTRA SONO GRAPHY

PICTORIAL ESSAY

https://doi.org/10.14366/usg.21189
pISSN: 2288-5919 • eISSN: 2288-5943
Ultrasonography 2022;41:416-429

Ultrasonography (US) is widely used for abdominal imaging. Its noninvasiveness, extensive range of application, and low cost make US a useful and valuable tool for the detection, diagnosis, and follow-up of splenic abnormalities. Concomitantly with the increasing frequency of imaging, more splenic lesions are being discovered and the requirements for the differential diagnosis are rising. In this pictorial essay, we introduce the representative US findings of many different splenic lesions, including normal sonographic findings, normal variants and congenital anomalies, infectious conditions, benign and malignant neoplasms, and non-neoplastic lesions. Knowledge of the US features of various splenic lesions will help narrow the differential diagnosis and guide clinical decision-making.

Keywords: Ultrasonography; Spleen; Splenic neoplasms; Splenic infarction; Splenic diseases
Key points: Ultrasonography is a useful and valuable tool for the detection, diagnosis, and follow-up of splenic abnormalities.

Received: September 8, 2021
Revised: December 1, 2021
Accepted: December 2, 2021

Correspondence to:
Kyeong Ah Kim, MD, PhD, Department of Radiology, Korea University Guro Hospital, Korea University College of Medicine, 148 Gurodong-ro, Guro-gu, Seoul 08308, Korea

Tel. +82-2-2626-1338
Fax. +82-2-863-9282
E-mail: kahkim@korea.ac.kr

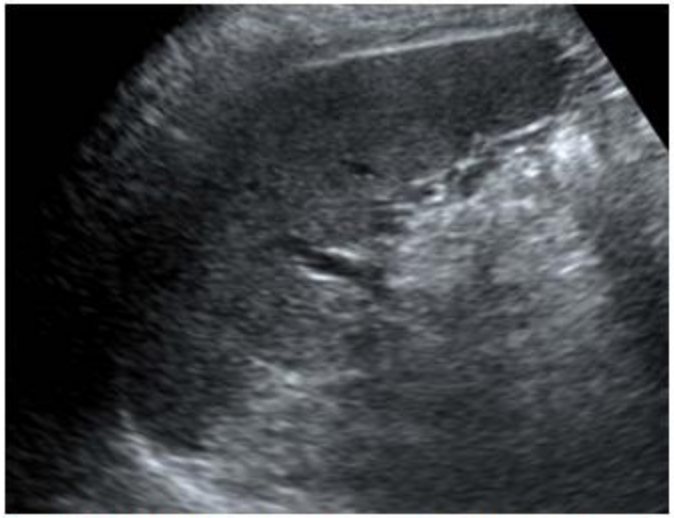

Fig. 1. **A 49-year old man with a normal-appearing spleen on ultrasonography (US).** Longitudinal US of the normal spleen shows homogeneous and uniform parenchymal echogenicity, and a crescent shape with smooth outer convexity and nodulous inner margin.

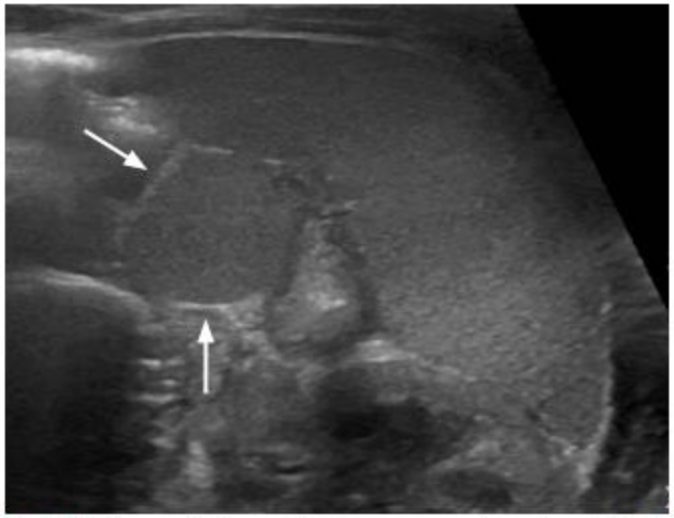

Fig. 2. **A 3-year-old boy with an accessory spleen.** Longitudinal ultrasonography of the spleen shows an approximately 1.2-cm round to oval mass (arrows) with echogenicity identical to that of the spleen at the splenic hilum, suggesting an accessory spleen.

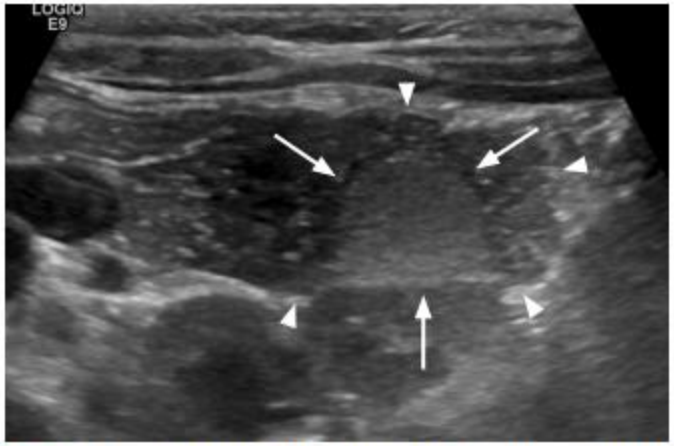

Fig. 3. **A 6-year-old girl with an intrapancreatic accessory spleen (IPAS).** Transverse ultrasonography of the pancreas shows a 1.3-cm round to oval echogenic mass (arrows) in the pancreas tail (arrowheads), with echogenicity that is identical to that of the splenic parenchyma, suggesting IPAS.

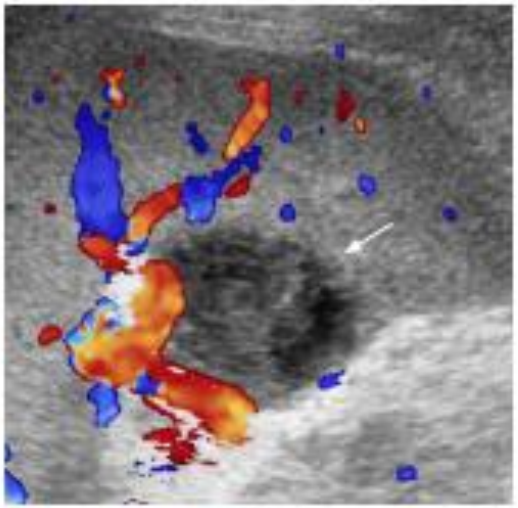

Fig. 3. A 60-year-old woman with pyogenic abscess of the spleen.
Longitudinal ultrasonography (US) of the spleen shows an oval heterogeneous hypoechoic lesion (arrow) with mild acoustic enhancement in the splenic hilum suggesting an abscess. Klebsiella pneumoniae was identified in US-guided aspiration.

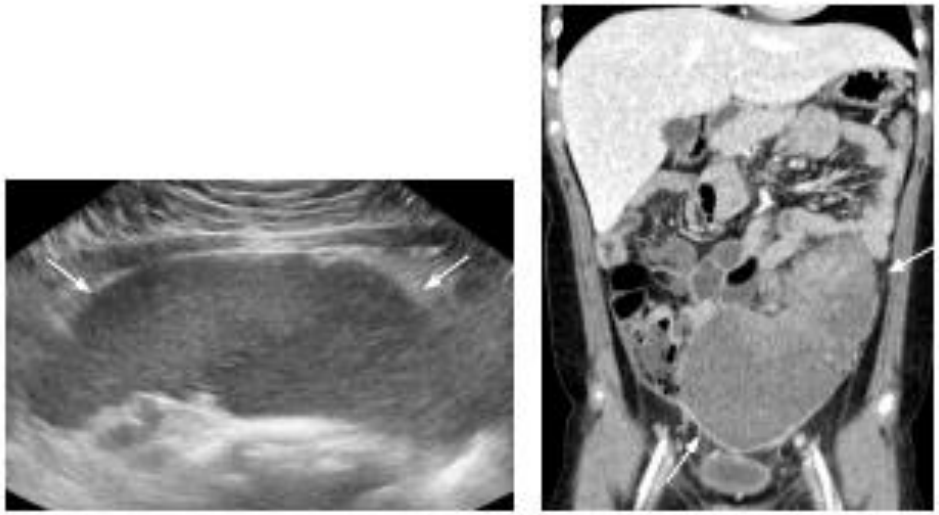

A B

Fig. 4. An 8-year-old girl with a wandering spleen.
A. Transverse ultrasonography of the lower abdomen shows a crescent-shaped homogeneous abdominal mass (arrows) suggesting that the spleen is in an unusual anatomical location, a condition known as "wandering spleen." In this patient, the ectopic spleen was enlarged and the parenchymal echogenicity was heterogeneous. B. Follow-up computed tomography scan of the same patient with abdominal pain shows torsion and ischemia of the wandering spleen (arrows).

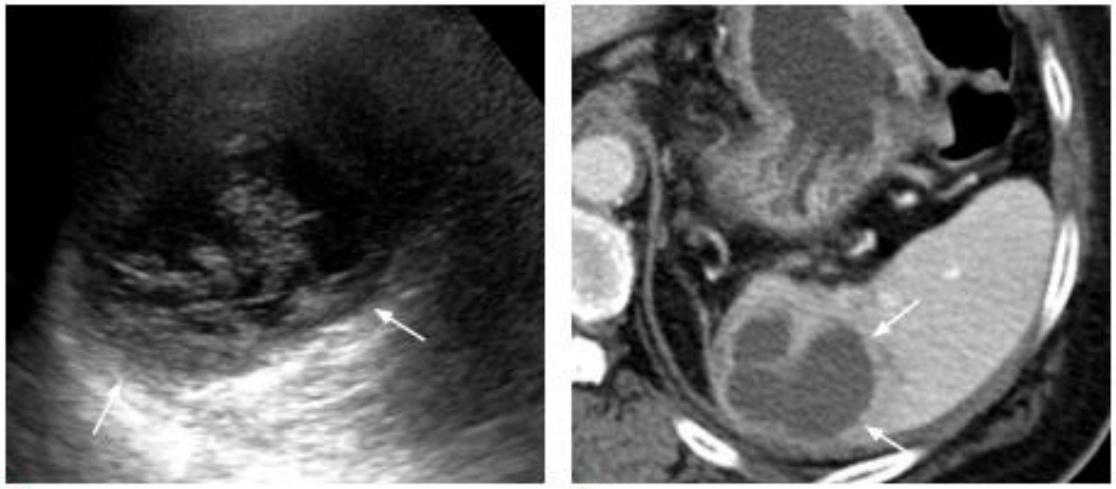

A B

Fig. 6. A 65-year-old woman with pyogenic abscess of the spleen.
A. Longitudinal ultrasonography (US) of the spleen shows a poorly defined round anechoic cystic mass (arrows) with echogenic internal debris suggestive of an abscess. *Salmonella* group D was identified by US-guided aspiration. B. Axial contrast-enhanced computed tomography image shows a rim-enhancing multiseptated hypodense lesion (arrows) in the spleen.

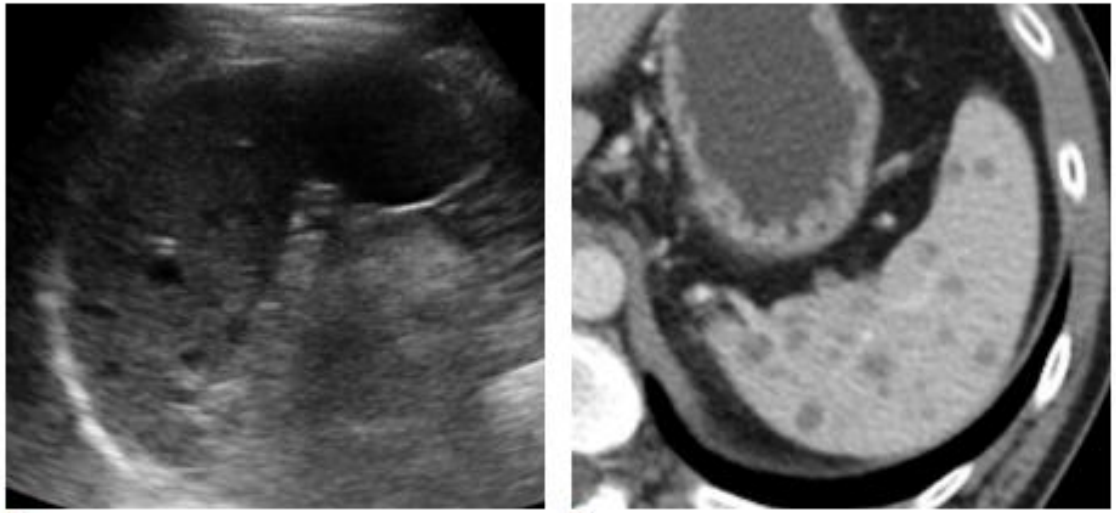

A B

Fig. 7. A 35-year-old human immunodeficiency virus–positive man with miliary tuberculosis infection of the spleen.
A. Longitudinal ultrasonography (US) of the spleen shows multiple small (<1 cm) hypoechoic lesions in the splenic parenchyma. US-guided biopsy confirmed the presence of Mycobacterium tuberculosis. B. Axial contrast enhanced computed tomography image shows numerous, subcentimeter, hypodense nodular lesions throughout the spleen.

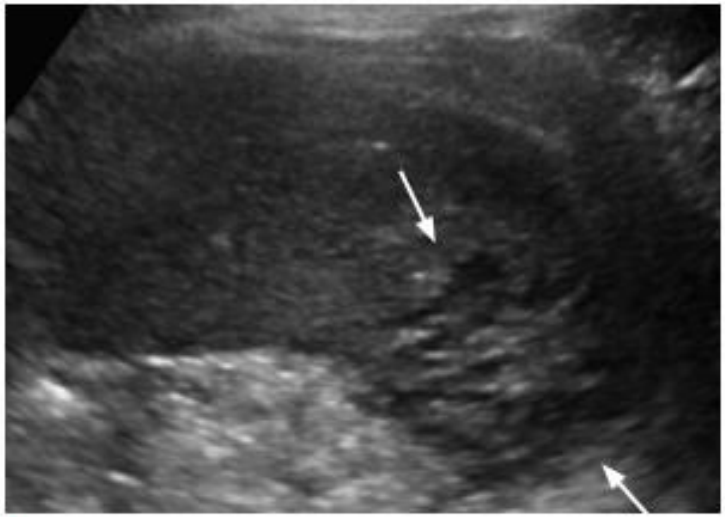

A

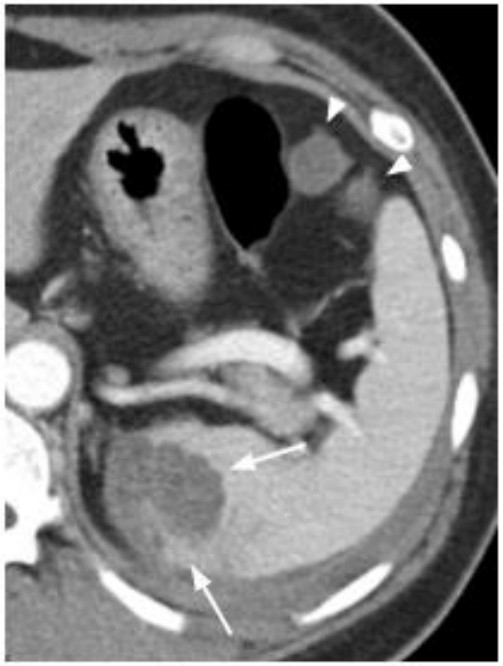

B

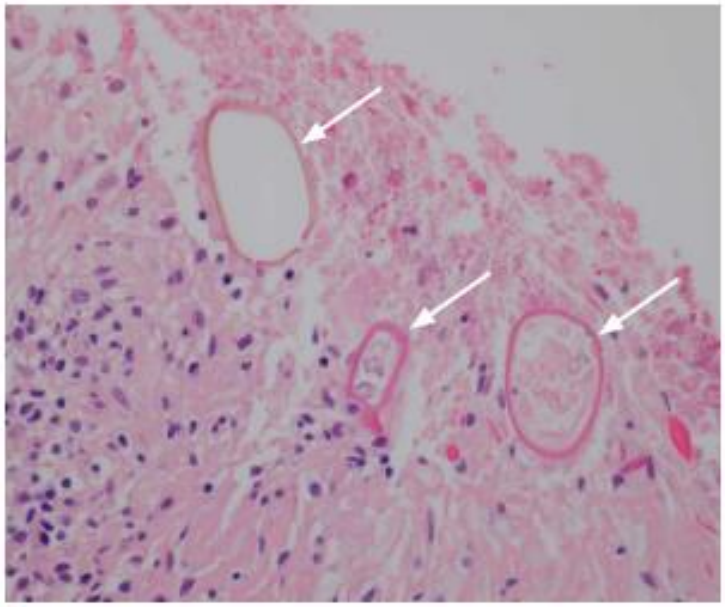

C

Fig. 8. **A 44-year-old woman with paragonimiasis.**
A. Longitudinal ultrasonography (US) of the spleen shows an approximately 3.5-cm clustered multicystic lesion (arrows). US-guided biopsy confirmed eggs from *Paragonimus westermani*. B. Axial contrast-enhanced computed tomography image shows a lobulated hypodense splenic lesion with clustered multiple cysts (arrows). Two small peritoneal cystic lesions (arrowheads) and left pleural effusion were also observed. C. Microscopic image with hematoxylin and eosin staining (×400) shows the ovoid parasite eggs with a thick shell (arrows) in necrotic splenic tissue, morphologically consistent with *P. westermani*.

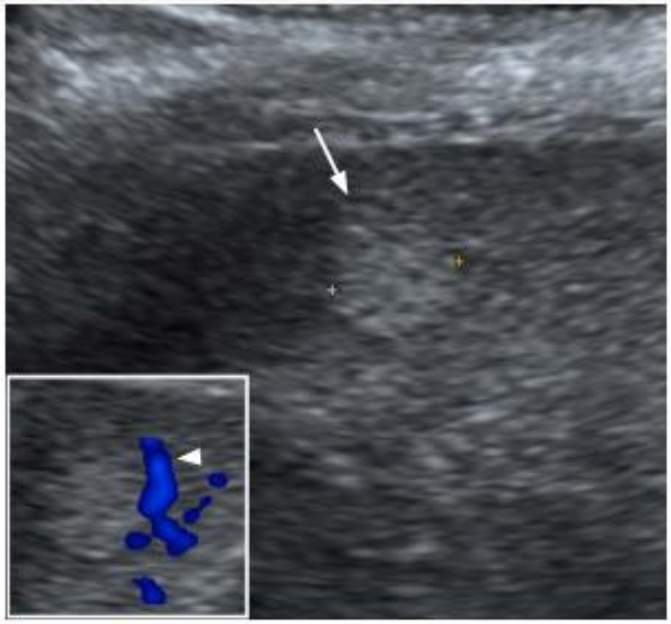

A

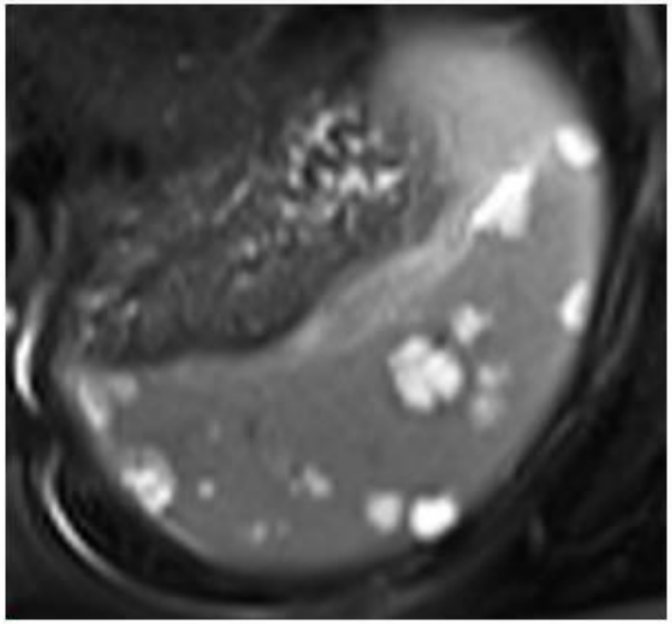

B

Fig. 9. **A 33-year-old woman with a splenic hemangioma.**
A. Longitudinal ultrasonography (US) of the spleen shows an incidentally found, discrete, round, echogenic nodule (arrow). Color Doppler US (box) showed peripheral vascularity (arrowhead) of the nodule. B. Axial magnetic resonance imaging; a T2-weighted image shows multiple well-defined, round, T2 high-signal-intensity lesions suggestive of hemangiomas.

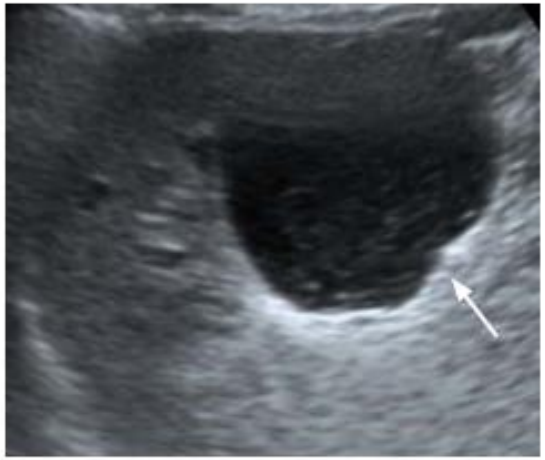

A

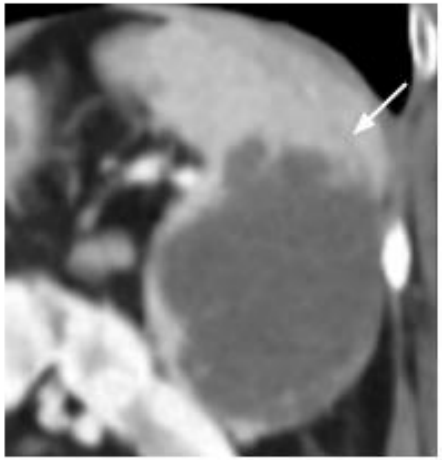

B

Fig. 10. **A 61-year-old woman with a splenic hemangioma.**
A. Longitudinal ultrasonography of the spleen shows a lobulated cystic lesion (arrow) at the splenic inferior pole with an internal echogenic solid portion. B. Coronal contrast-enhanced computed tomography image shows a lobulated low-density lesion (arrow) in the splenic inferior pole.

A

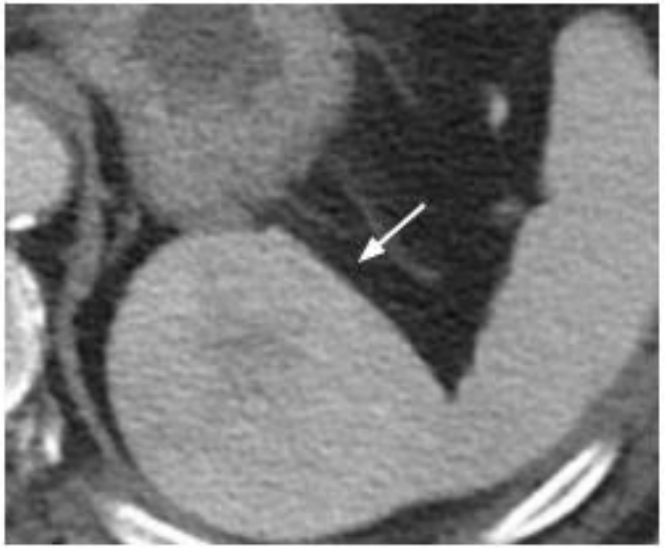

B

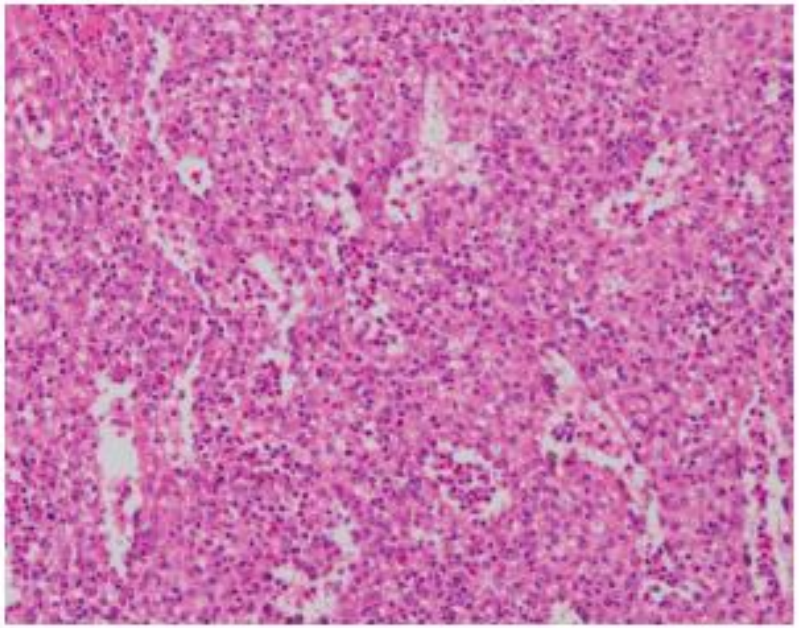

C

Fig. 11. A 70-year-old man with a splenic hamartoma.
A. Longitudinal ultrasonography of the spleen shows an approximately 5-cm, homogeneously isoechoic round mass (arrow) in the splenic upper pole. B. Axial contrast-enhanced computed tomography image shows a heterogeneously enhancing round mass (arrow) in the spleen, which was confirmed to be a hamartoma. C. Microscopic image with hematoxylin and eosin stain (×100) shows disorganized blood vessels of varying sizes intermingled with splenic red pulp.

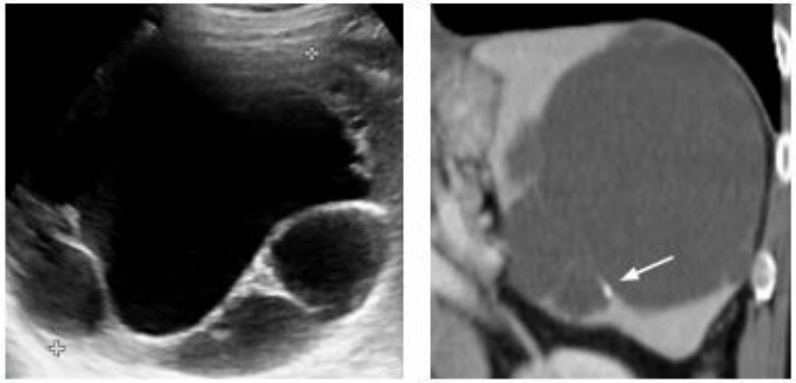

A B

Fig. 12. A 74-year-old woman with splenic lymphangioma.
A. Transverse ultrasonography of the spleen shows an incidentally observed multiloculated cystic lesion measuring approximately 12 cm in the splenic upper pole. B. Coronal contrast-enhanced computed tomography image shows a multiloculated large cystic lesion with thin-wall calcification (arrow).

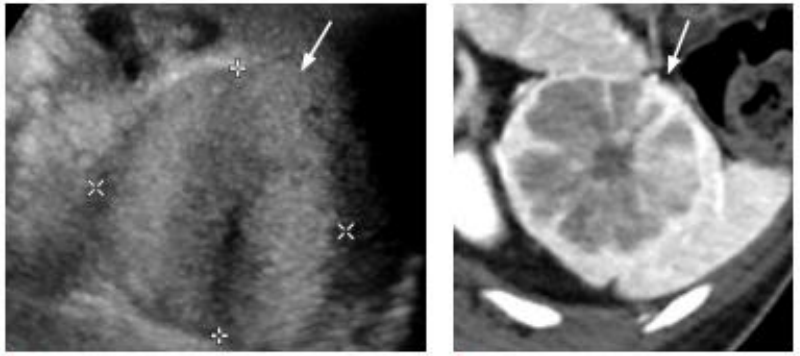

A B

Fig. 13. A 51-year-old woman with splenic sclerosing angiomatoid nodular transformation (SANT).
A. Longitudinal ultrasonography of the spleen shows an approximately 5 cm × 4 cm well-defined oval echogenic mass (arrow). B. Axial image of contrast-enhanced computed tomography shows the characteristic "spoke wheel" appearance (arrow) suggesting SANT.

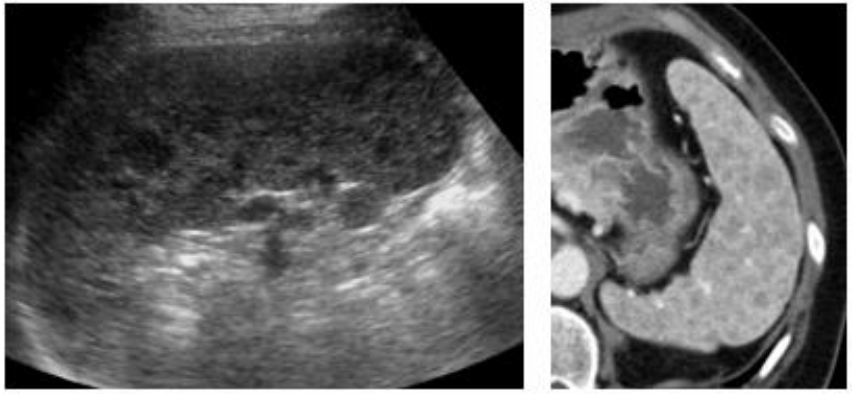

A B

Fig. 14. A 56-year-old woman with diffuse large B-cell lymphoma (DLBCL).
A. Longitudinal ultrasonography (US) of the spleen shows numerous conglomerated hypoechoic nodules. B. Axial contrast-enhanced computed tomography image shows numerous hypodense nodules in the spleen. US-guided biopsy confirmed DLBCL involvement of the spleen.

Fig. 15. **A 6-year-old boy with systemic Epstein–Barr virus-positive T-cell lymphoma of childhood.** Longitudinal ultrasonography of the spleen shows a heterogeneously hypoechoic mass (arrow) with splenomegaly (11.5 cm).

avascular on color Doppler US [17].

Angiosarcoma

Angiosarcoma is the most common primary nonhematopoietic malignant neoplasm of the spleen. It is highly malignant and develops from the endothelial lining of blood vessels in spleen. On US, it is seen as well-defined heterogeneous solitary or multiple nodules or masses with hemorrhagic or necrotic changes, or splenomegaly in diffusely infiltrative cases [1,2]. In color Doppler US, increased blood flow may be seen in the hyperechoic solid portion [5,12].

Non-neoplastic Lesions

Splenomegaly

Splenomegaly can be diagnosed in patients with acute or chronic splenic enlargement, with splenic length >11–12 cm and width

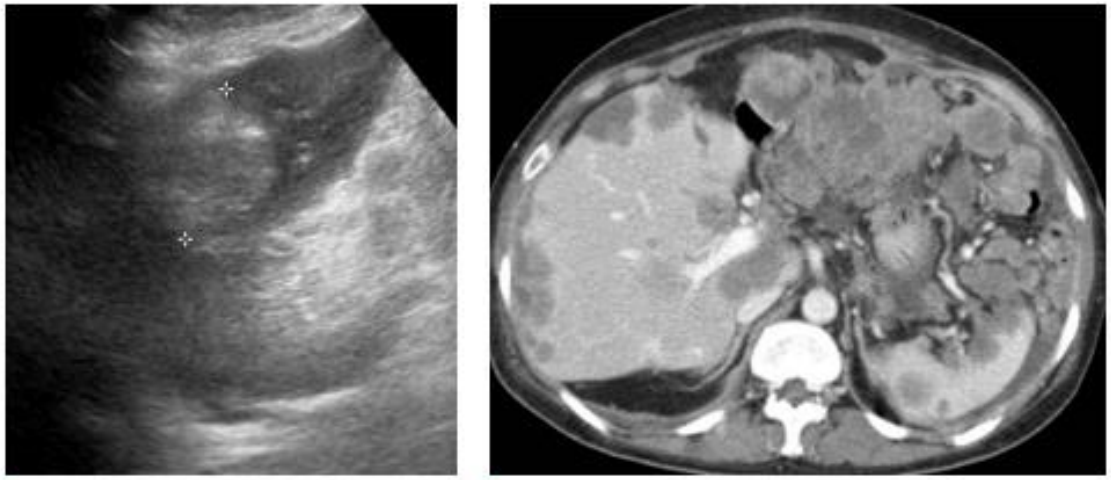

A B

Fig. 16. **A 48-year-old woman with rectal cancer with multiple metastases including splenic metastasis and peritoneal carcinomatosis.** A. Longitudinal ultrasonography of the spleen shows a round echogenic mass suggestive of metastasis. B. Axial contrast-enhanced computed tomography image shows multiple metastases to the liver, spleen, lymph nodes, and peritoneal carcinomatosis.

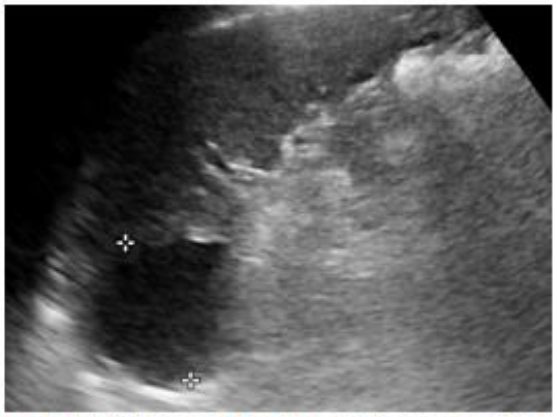

Fig. 18. **An 83-year-old man with a splenic cyst.** Longitudinal ultrasonography of the spleen shows an approximately 4-cm well-defined round anechoic cystic lesion at the splenic upper pole.

A

B

Fig. 17. **A 33-year-old man with splenomegaly and alcoholic hepatitis.**
A–C. Longitudinal ultrasonography of the spleen (A), abdominal plain radiograph (B), and axial abdominal computed tomography image (C) shows splenomegaly (>21cm in length, arrows in B indicate enlarged splenic shadow).

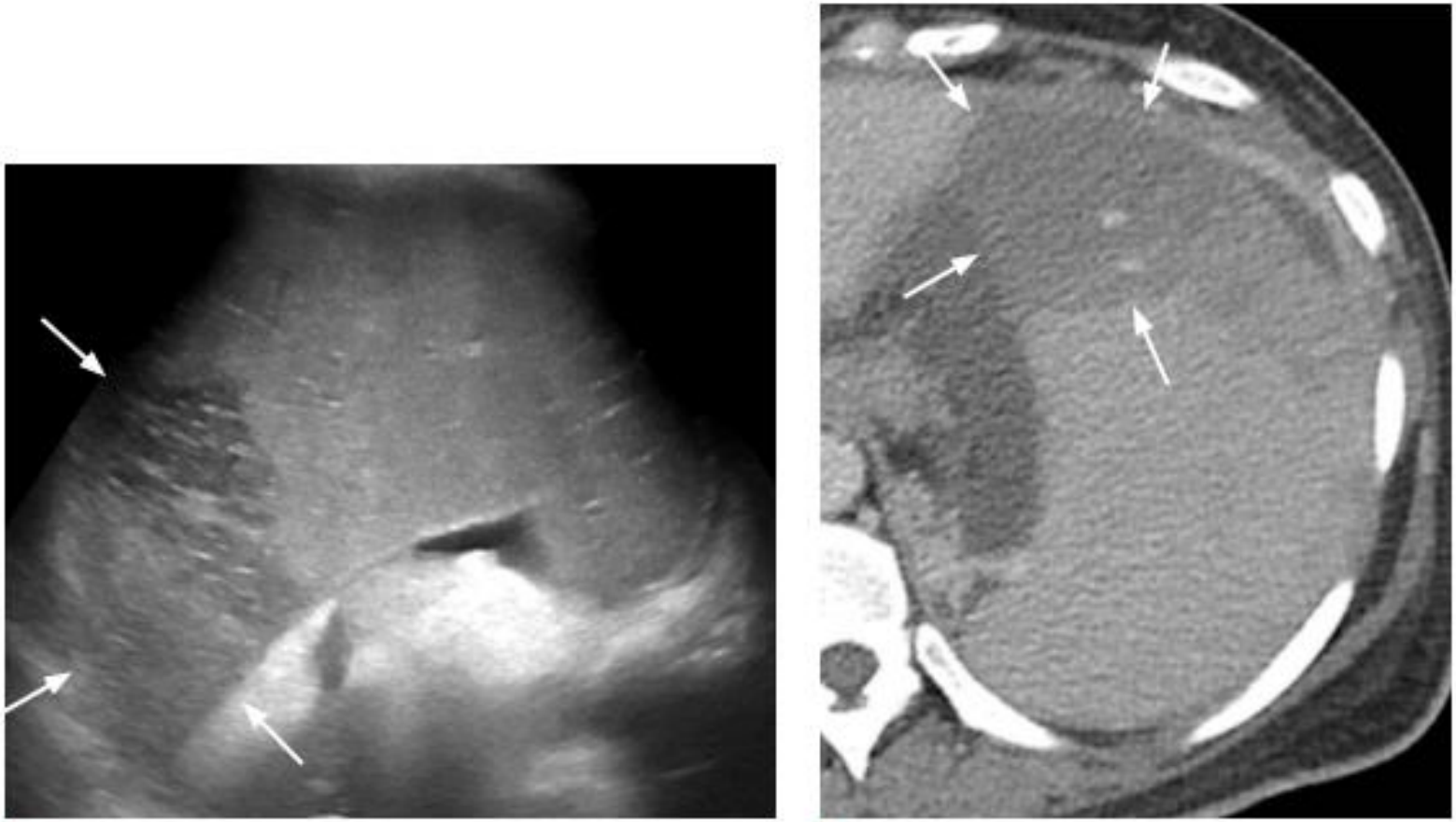

A B

Fig. 19. A 41-year-old woman with splenic infarction and underlying liver cirrhosis and splenomegaly.
A. Longitudinal ultrasonography (US) of the spleen shows a well-defined hypoechoic area (arrows) in the enlarged spleen. B. Axial contrast-enhanced computed tomography image shows a wedge-shaped hypoenhancing area (arrows) in the enlarged spleen, which matched the US findings.

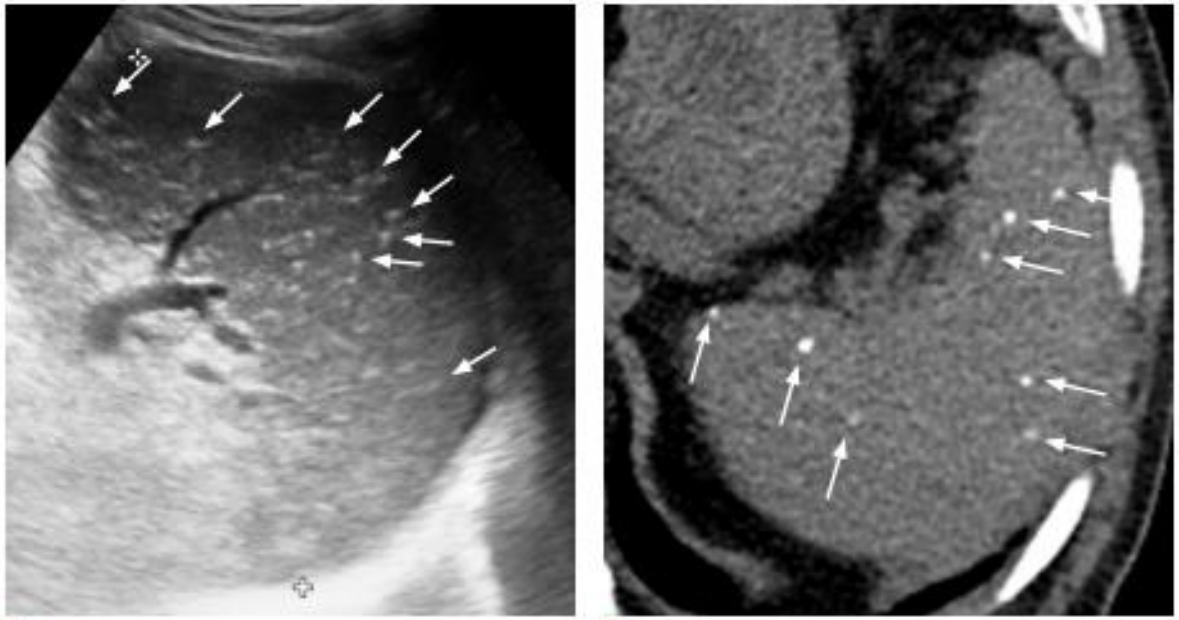

A B

Fig. 20. **A 63-year-old man with Gamna-Gandy bodies in the spleen.**
A. Longitudinal ultrasonography of the spleen shows numerous scattered tiny punctate hyperechoic foci (arrows). B. Axial non-enhanced computed tomography image shows multiple tiny calcifications (arrows) in the spleen.

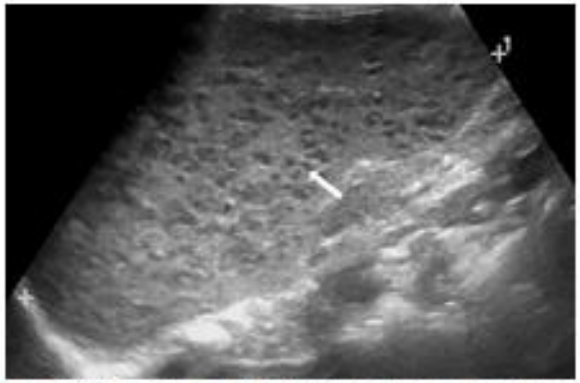

Fig. 21. **A 3-year-old girl with splenic peliosis.** Longitudinal ultrasonography of the spleen shows splenomegaly and multiple poorly defined hypoechoic nodules (arrow).

US of the spleen is readily performed as part of abdominal imaging, and the detection of splenic lesions is increasing. However, the differential diagnosis is challenging because a single disease category of the spleen can show various US findings, while many different splenic lesions have overlapping US findings. Table 2 presents a summary of the US findings of various splenic lesions. Most infectious and inflammatory lesions are seen as multiple small hypoechoic lesions, pyogenic abscesses have thick irregular walls, and parasitic infections typically show cystic lesions. Splenic hemangiomas have similar US features to hepatic hemangiomas. Hamartomas are typically isoechoic to hyperechoic on grayscale US and hypervascular on color Doppler US. Lymphangiomas are seen as thin-walled multilocular cysts. Lymphomas show various US features, ranging from solid nodules or masses to a miliary pattern and diffuse infiltration. Metastatic lesions in the spleen also show variable findings depending on the primary malignancy. Angiosarcoma shows splenomegaly with diffuse infiltration or multiple heterogeneous masses. Splenic infarction, for which various predisposing conditions have been identified, is seen as a wedgeshaped hypoechoic area. US examinations of the spleen can help narrow down the differential diagnosis and provide ancillary findings of the patient's condition. Moreover, US-guided biopsy of the target lesion in the spleen facilitates a minimally invasive and confirmative diagnosis.

Table 2. Summary of various splenic lesions on US

	Solitary/multiple/ diffuse	Splenomegaly	US	Color Doppler US	Clues
Normal variants and congenital abnormalities					
Accessory spleen	Solitary, multiple	N/A	Echogenicity identical to normal spleen	Vascular hilum arising from splenic vessels	Round to oval mass at splenic hilum
IPAS	Solitary	N/A	Echogenicity identical to normal spleen	Vascular supply from splenic artery	Usually have fibrotic capsule
Wandering spleen	Solitary	N/A	Torsion (+): hypoechoic	Torsion (+): decreased flow	Unusual location torsion (+): twisted vascular pedicle
Infections and splenic abscess					
Pyogenic abscess	Solitary, multiple	Variable	Thick walled, irregular anechoic/ hypoechoic cyst	Absent internal flow	–
Fungal infection	Multiple	Variable	Hypoechoic microabscesses	Absent internal flow	Immunocompromised
Mycobacterial abscess	Multiple, solitary	+	Hypoechoic	Nonspecific	Associated lymphadenopathy
Parasitic infection	Multiple	Variable	Anechoic cyst	Nonspecific	Daughter cysts, clusters of small cysts
Benign neoplasms					
Hemangioma	Solitary, multiple (hemangiomatosis)	–	Small: echogenic Large: complex solid and cystic	Intralesional, peripheral flow/avascular	Similar to hepatic hemangioma
Hamartoma	Solitary, multiple (hamartomatosis)	–	Homogeneous isoechoic to hyperechoic	Hypervascular	–
Lymphangioma	Solitary, multiple (lymphangiomatosis)	Variable	Multilocular cyst	Mural vascularity	–
SANT	Solitary, multiple	–	Heterogeneous mass with hyperechoic septae	Arterial flow	–
Malignant neoplasms					
Lymphoma	Solitary, multiple, diffuse	+	Various	Avascular	–
Metastases	Solitary, multiple, diffuse	– (possible in diffuse)	Various	Avascular	–
Angiosarcoma	Diffuse, solitary, multiple	+	Heterogeneous	Hypervascular solid portion	–
Non-neopalstic lesions					–
Congenital cyst	Solitary	Variable	Anechoic cyst	Avascular	–
False cyst or pseudocyst	Solitary	Variable	Anechoic cyst±internal debris	Avascular	–
Splenic infarction	Solitary, multiple	–	Hypoechoic (acute), becoming hyperechoic	Avascular	Wedge-shaped hypoechoic area
Gamna-Gandy bodies	Multiple	+ (associated with cirrhosis)	Punctate hyperechoic foci	Avascular	Organized hemorrhagic infarcts
Peliosis	Multiple	Variable	Poorly defined hypoechoic lesions	Intralesional flow/ avascular	–

US, ultrasonography; N/A, not applicable; IPAS, intrapancreatic accessory spleen; SANT, sclerosing angiomatoid nodular transformation.